






 Cite this: *RSC Adv.*, 2021, 11, 30827

Bis-indolylolation of aldehydes and ketones using silica-supported FeCl₃: molecular docking studies of bisindoles by targeting SARS-CoV-2 main protease binding sites†

 Barnali Deb, ^a Sudhan Debnath, ^{*b} Ankita Chakraborty ^{‡a} and Swapan Majumdar ^{*a}

We report herein an operationally simple, efficient and versatile procedure for the synthesis of bis-indolylmethanes *via* the reaction of indoles with aldehydes or ketones in the presence of silica-supported ferric chloride under grindstone conditions. The prepared supported catalyst was characterized by SEM and EDX spectroscopy. The present protocol has several advantages such as shorter reaction time, high yield, avoidance of using harmful organic solvents during the reaction and tolerance of a wide range of functional groups. Molecular docking studies targeted toward the binding site of SARS-CoV-2 main protease (3CL^{PRO} or M^{PRO}) enzymes were investigated with the synthesized bis-indoles. Our study revealed that some of the synthesized compounds have potentiality to inhibit the SARS-CoV-2 M^{PRO} enzyme by interacting with key amino acid residues of the active sites *via* hydrophobic as well as hydrogen bonding interactions.

 Received 25th July 2021
 Accepted 1st September 2021

DOI: 10.1039/d1ra05679d

rsc.li/rsc-advances

Introduction

Giving high priority to social responsibility and public awareness to conserve our mother nature, the synthetic organic chemistry community designs any chemical process in such a way so that it can eliminate or reduce the use of harmful chemicals as much as possible during manufacturing and processing to keep the environment clean and sustainable for future generations. Therefore, the development of efficient and environmentally benign synthetic strategies is the prime task of organic chemists in academic and industrial settings.¹ Thus, over the last decade, tremendous efforts have been devoted to the exploration of an eco-friendly methodology in both academia and industries using solvent-free techniques,² ionic liquids,³ water media,⁴ phase transfer catalysts,⁵ solid-supported catalysts,⁶ microwave irradiation⁷ or grindstone/ball-milling processes.⁸ The use of grindstone chemistry is very fascinating for the synthesis of desired functional molecules *via* simple mixing of the precursors and catalysts with much faster reaction rates and selectivity under benign reaction

conditions. In recent times, much attention has been paid to organic transformations promoted by solid-supported reagents or catalysts and till now they occupy a special position in the development of greener chemical processes due to their attractive properties such as high surface area, crystalline structure, less or no corrosion, high thermal stability, persistence in all organic solvents, no waste or disposal problems, and recyclability. Among various solid supports, silica gel is one of the extensively used surface material⁹ for different chemical transformations in organic chemistry, as it displays many significant advantages such as high surface area, thermal and chemical stability, easy availability, low cost and insolubility in organic solvents. Recently, silica-supported ferric chloride has been used as an efficient heterogeneous catalyst in many organic transformations by us^{10a} and others^{10b-e} in different occasions.

The indole scaffold has been recognized as a prominent and privileged structural motif found in thousands of natural products, exhibiting a range of important biological activities and gaining technological interest.¹¹ Many indole derivatives were found to possess anti-inflammatory activity along with analgesic and antipyretic properties. They inhibit the production of eicosanoids such as prostacyclin, thromboxanes and prostaglandins *via* inhibiting cyclooxygenase activity and thereby reduce edema. Indole analogues are the most important series of inhibitors with considerable anti-viral activities against hepatitis C virus (HCV), acting at a non-structural 5B RNA-dependent-RNA-polymerase (RdRp) thumb site I.¹² Three

^aDepartment of Chemistry, Tripura University, Suryamaninagar, 799 022, India. E-mail: smajumdar@tripurauniv.ac.in; Fax: +91-381-237-4802; Tel: +91-381-237-9070

^bDepartment of Chemistry, Netaji Subhash Mahavidyalaya, Tripura, 799114, India

† Electronic supplementary information (ESI) available. See DOI: 10.1039/d1ra05679d

‡ Present address: Department of Chemistry, Faculty of Science and Technology, ICFAI University/Tripura, Kamalghat, Mohanpur, Agartala, Tripura 799210.



compounds, namely, indigo, indirubin, and indicant containing an indole moiety isolated from the roots of the plant *Isatis indigotica* were tested against SARS-CoV 3CL^{pro}, and they showed inhibitory activity on cell-free cleavage of SARS-CoV 3CL^{pro} and their IC₅₀ values were 37.3, 81.3 and 33.1 μg mL⁻¹ respectively.¹³ Another indole derivative, 5-chloropyridin-3-yl-1*H*-indole-4-carboxylate showed excellent SARS-CoV 3CL^{pro} inhibitory activity with an IC₅₀ value of 30 nM.¹⁴ Arbidol, a small indole derivative, showed broad spectrum activity against influenza and other respiratory viral infections.¹⁵ It has a capacity to interact with both membrane and viral cellular proteins. The above-mentioned evidence indicates that indole derivatives act as anti-viral agents. Zhang *et al.* in their comprehensive overview on indole derivatives also highlighted the anti-viral activities of indole derivatives.¹⁶ They also promote the idea that indole macrocycles such as bis- and tris-indole may be exploited in future as novel lead compounds for use as anti-viral agents. Indole or its derivatives are also known as versatile intermediates in organic synthesis due to the feasibility of the 3-position of indole for electrophilic substitution.¹⁷ Consequently, 3-substituted indoles were carefully screened for components of drugs and are generally found to be of pharmaceutical interest in a variety of therapeutic areas. Bis(indolyl) methanes (BIMs) are a group of alkaloids with a basic skeleton of two indoles bridged by single methyl carbon; they are differentiated by the groups/substituents attached to the bridging methyl carbon (Fig. 1, 1).¹⁸ Several bis(indolyl) methanes and their derivatives have been isolated from terrestrial and marine natural sources, namely, parasitic bacteria, tunicates, and sponges, and some of these possess significant biological activities.¹⁹ The natural bis-indolylmethane (Fig. 1, I–V) and some of its analogues exhibit antibacterial, antifungal, anticancer and immunostimulatory properties including anti-pyretic, anti-inflammatory, anthelmintic, cardio-vascular, anti-convulsant, antimicrobial and selective COX-2 inhibitory activities. Bis(indol-3-yl) methanes (BIMs) and their oxidized derivatives are useful as dyes,²⁰ colorimetric chemosensors,²¹ fluorescent chemosensors for Cu²⁺ cation²² and sensors of aspartate and glutamate.²³

The acid-catalyzed reaction of electron-rich heterocyclic compounds such as indoles and pyrroles with *p*-dimethyl aminobenzaldehyde is known as the Ehrlich test.²⁴ Generally, 3,3'-bis(indolyl) methanes are synthesized by an analogous reaction to the Ehrlich test, where indole reacts with aldehydes or

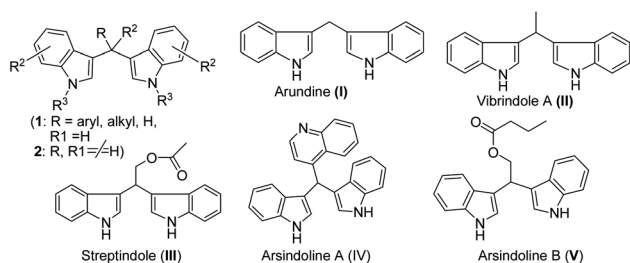
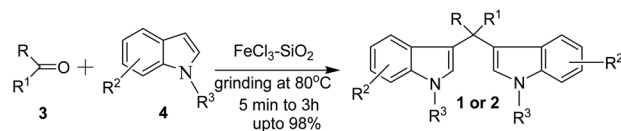


Fig. 1 Bis(indolyl) methane and some naturally occurring bis-indolylmethane alkaloids.



Scheme 1 General strategy for the synthesis of BIMs under solvent-free SiO₂-FeCl₃ catalysis.

ketones in the presence of an acid catalyst to produce an azafulvenium salt, which undergoes further addition reaction with a second indole molecule to produce bis(indolyl) methanes. The role of protic acid or Lewis acid is basically activation of carbonyl and the formation of azafulvenium ions. Except Ehrlich test-type condensation, other approaches for BIM synthesis, *e.g.* transition metal-catalysed oxidative coupling,²⁵ Bartoli-type reaction²⁶ and photoredox-catalysed ring opening functionalization of tetrahydroisoquinolines²⁷ are known. However, due to the wide substrate and reagent scopes of Ehrlich test-type acid-catalysed electrophilic substitution reaction of indoles with aldehydes, it is one of the widely acceptable simple and straightforward approaches for the synthesis of bis-indolylmethanes. Consequently, several methods have been reported for the synthesis of these compounds. A variety of reagents such as protic acid,²⁸ Lewis acids,²⁹ transition and non-transitional metal salts,³⁰ solid acidic catalysts³¹ and ionic

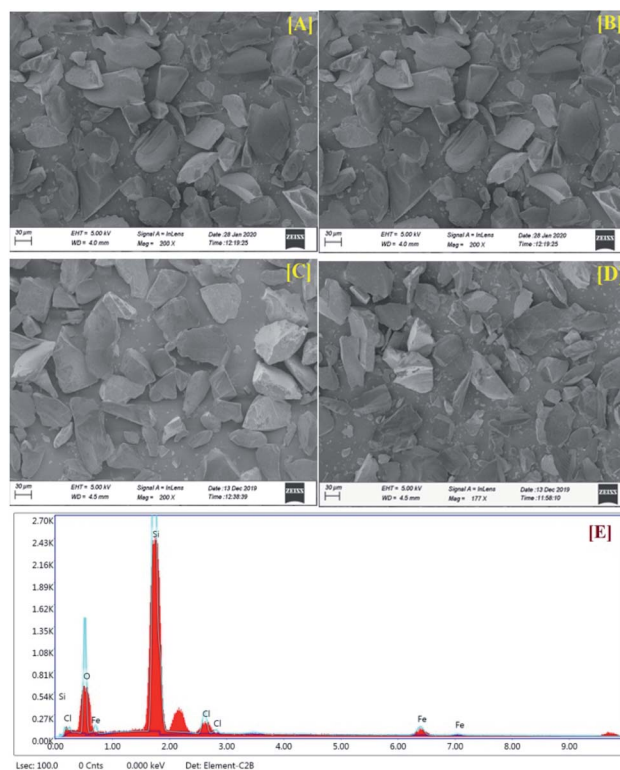


Fig. 2 Chtrs characterisation of the SiO₂-FeCl₃ catalyst: [A] SEM images of SiO₂ of 230–400 mesh, [B] SEM images of freshly prepared SiO₂-FeCl₃, [C] six-month-old SiO₂-FeCl₃, [D] recycled SiO₂-FeCl₃ and [E] EDAX spectrum of SiO₂-FeCl₃ showing absorption peaks for Fe, Cl, Si and O.

liquids³² have been employed to accomplish this transformation. However, many of these methods suffer from disadvantages such as unsatisfactory yields, expensive catalysts, long reaction times, toxic organic solvents, laborious work-up procedures, requirement of special apparatus, and harsh reaction conditions. Thus, the development of simple, efficient, high-yielding, and eco-friendly methods using new recyclable catalysts for the synthesis of these compounds would be highly desirable. With the purpose to develop more efficient synthetic processes, reduce the number of separate reaction steps and minimize the by-products, herein we report a novel and efficient method for the preparation of bis-indolylmethane derivatives (BIM's) *via* multi-component assembly of indoles and aldehydes in the presence of silica-supported ferric chloride (SiO₂-FeCl₃) as an efficient, non-volatile, recyclable, easy-to-handle and eco-friendly catalyst (Scheme 1). Furthermore, molecular docking studies of the synthesized compounds were also performed to understand their binding affinities towards M^{Pro}, a crucial life cycle enzyme of SARS-CoV-2.

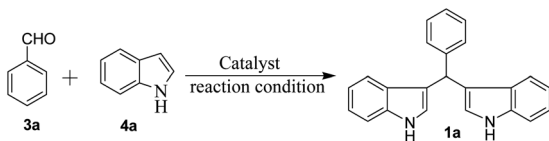
Silica-supported ferric chloride (FeCl₃/SiO₂) was first prepared by Mazur and Keinan^{10b} who used it as a Lewis acid to dehydrative rearrangement of alcohols. We prepared the same with slight modifications in the procedure and characterized the supported catalyst by SEM analysis. Typically, to the slurry of silica gel (240–300 mesh, 40 g) in acetone (80 mL), anhydrous ferric chloride (5 g, 30.83 mmol) was added with vigorous stirring for 1 h. The excess acetone was removed under reduced pressure and then the mixture was dried under vacuum (~1 mm

Hg) for 24 h to obtain a free flowing solid. The catalyst was stored in a brown colour bottle at 4 °C for longer shelf life. SEM micrographs of the silica, and freshly prepared, six-month-old and recovered catalyst are shown in Fig. 2(A)–(D). An EDX spectrum of the catalyst is shown in Fig. 2(E). The stability of the catalyst was also judged by EDX spectra of the six-month-old catalyst and the recovered catalyst indicated that the quality of the catalyst do not deteriorate even after five cycles (ESI†).

Results and discussion

To optimize the reaction conditions for the synthesis of bis-indolylmethanes, we began with benzaldehyde (**3a**) and indole (**4a**) as model substrates using different amounts of catalysts under grindstone conditions. No product was obtained upon grinding of **3a** and **4a** in a 1 : 2 molar ratio in the absence of the catalyst (Table 1, entry 1), but at elevated temperatures, very little conversion was observed (Table 1, entry 2). However, grinding with chromatographic grade silica facilitated the reaction to yield 70% of **1a** (Table 1, entry 3). Having in mind the Lewis acid character of FeCl₃, we have employed 5 mol% of FeCl₃ while grinding the mixture (Table 1, entry 4). Unfortunately, highly colored mixture of products (TLC) were obtained with full consumption of starting materials. We were pleased to observe that grinding the mixture with pre-prepared FeCl₃-SiO₂ (20 mg, containing 2 mol% of FeCl₃) for 3 h provides clean transformation of the substrates to the desired product in 92% yield (Table 1, entry 5), but the reaction was much faster at

Table 1 Optimization of catalyst loading, effect of solvent and temperature on model reaction of BIM synthesis



Entry	Catalyst	Solvent	Temp (°C)	Time (min)	Yield ^a (%)
1	No	No	rt	120	NR
2	No	No	80	15	Mixture
3	SiO ₂	No	80	180	70
4	FeCl ₃	No	80	30	mixture
5	SiO ₂ -FeCl ₃ (2 mol% FeCl ₃) ^b	No	rt	180	92
6	SiO ₂ -FeCl ₃ (2 mol%)	No	80	5	96
7	SiO ₂ -FeCl ₃ (4 mol%)	No	80	5	96
8	SiO ₂ -FeCl ₃ (1 mol%)	No	80	20	92
9	SiO ₂ -FeCl ₃	CH ₂ Cl ₂	rt	15	84
10	SiO ₂ -FeCl ₃	EtOH	rt	90	87
11	SiO ₂ -KHSO ₄	No	80	10	65
12	SiO ₂ -HClO ₄	No	80	15	58
13	SiO ₂ -H ₂ SO ₄	No	80	10	78
14	Cu nano	No	80	90	90
15	Nano TS 1	No	80	40	50
16	Amberlite IR 120H ⁺	No	80	120	90
17	SiO ₂ -FeCl ₃ ^c	No	80	15	95

^a Isolated yield. ^b Calculated based on the amount of FeCl₃ used during preparation. ^c Reaction in 10 mmol scale.

80 °C, which afforded 96% of the yield of **1a** in 5 min (Table 1, entry 6). To evaluate the catalytic efficiency, we used different amounts of catalyst FeCl₃-SiO₂ in this condensation reaction (Table 1, entry 7 and 8). Increase in the amount of catalyst (4 mol%) did not improve further but decreases the amount of catalyst to 1 mol% and slightly decreases the yield of **1a**. SiO₂-FeCl₃ in the presence of solvent CH₂Cl₂ and EtOH at room temperature gave desired product in 84% and 87% of yield respectively within 15 min and 90 min (Table 1, entries 9 and 10). However, under identical conditions (Table 1, entry 6), other silica-supported catalysts such as SiO₂-KHSO₄, SiO₂-HClO₄, and SiO₂-H₂SO₄ have given bis(indolyl) product (**1a**) in 65%, 58%, and 78% of yield respectively (Table 1, entries 11–13). Furthermore, we also tested the catalytic activity of different nano catalysts such as Cu nanoparticles, nanoTitania Silica (TS 1) and resin-based catalyst Amberlite IR 120H+, which gave 90%, 50% and 90% of yield and the required time was 40–120 min (Table 1, entries 14–16). Amongst all, SiO₂-FeCl₃ was found to be an efficient catalyst for the synthesis of **1a**. The present protocol is also applicable for large-scale synthesis (10 mmol) of bis(indolyl) methane (entry 17), which gave 95% yield of **1a** in 15 min.

The scope of the current protocol was investigated by using a large variety of aldehydes and ketones with indoles. The aromatic aldehydes containing various substituents such as Me, OMe, OH, Cl, NMe₂, and NO₂ with simple or substituted indoles under the standard reaction condition (Table 1, entry 6) result in good to excellent yields of **1** (Fig. 3). From the results summarised in Fig. 3, it was observed that the required reaction time is little more in the case of electron-releasing substituents present in aromatic aldehyde (**1b–1g**) than in electron-withdrawing ones (**1o–1q**), which increases the reaction rate. In case of methyl substituents present in the indole ring (**1h** and **1j**), the reaction is completed within 5 min but –Br substituents present in position 5 of the indole moiety required little longer time, which may be due to the –I effect, but both gave excellent yields (**1i**). The presence of an electron-withdrawing nitro group in the indole scaffold took longer reaction times, which extend up to 45 min and yield of **1k** was found only 70%. This present method is equally effective for the synthesis of hetero aromatic bis(indolyl) methane compounds (**1l**, **1m**) and for long alkoxy chain containing bisindolyl methane derivatives (**1r**), in very good yield within 30–50 min reaction time. This reaction was further explored for the synthesis of tri-indolylmethane in high yields (**1n**) by the condensation of indol-3-carbaldehyde with two equivalents of indole under identical conditions. Interestingly, the catalyst was effectively used for the synthesis of 1,4-bis(di(1*H*-indol-3-yl)methyl)benzene (**1s**) and no mono product was detected under this reaction condition. The reaction of 4 equivalents of indole with 1 equivalent of terephthalaldehyde proceeded successfully to give the product (**1s**) in an excellent yield within 40–45 min. Next, we paid our attention towards the synthesis of bis-indolylmethane derivatives using aliphatic aldehydes and ketones. The aliphatic aldehydes such as acetaldehydes, butyraldehyde and glyoxal (40% aq) also reacted with indole under standardized reaction condition and yielded the corresponding

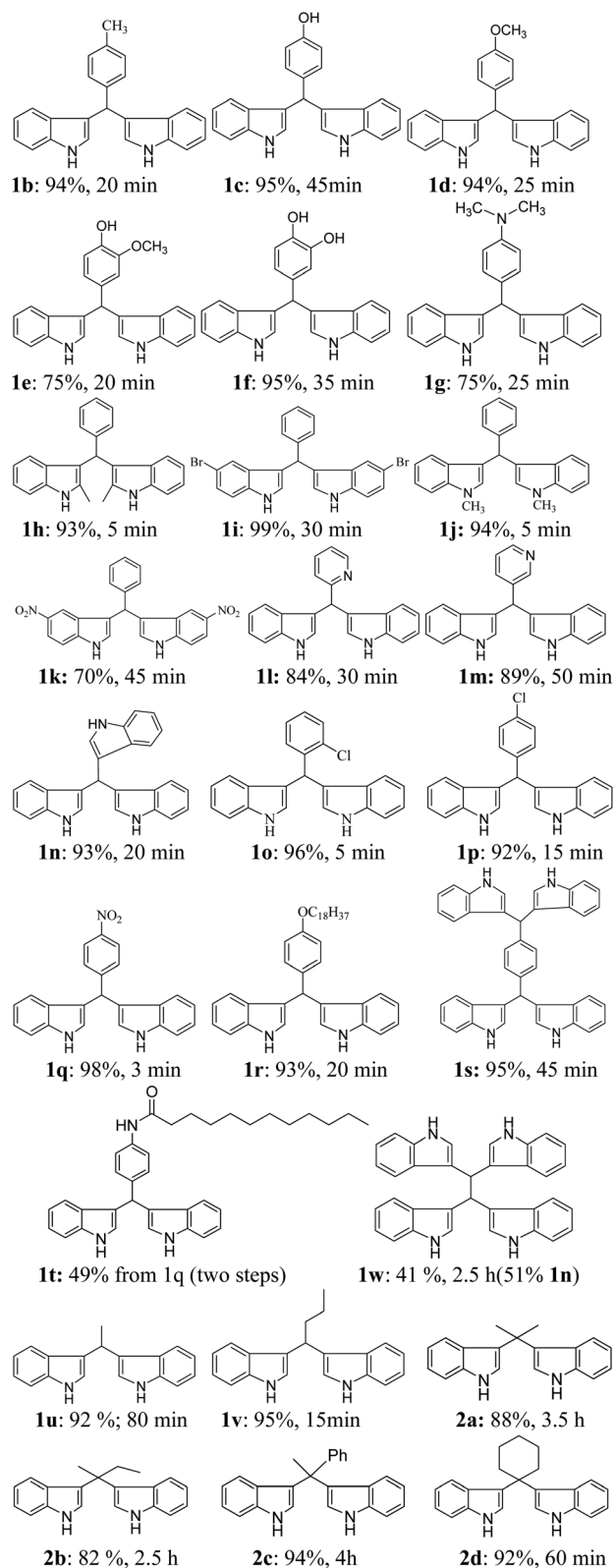


Fig. 3 Scope of aldehydes and aliphatic/aromatic ketones.



Fig. 4 Catalytic recyclability of $\text{SiO}_2\text{-FeCl}_3$ from the reaction between benzaldehyde and indole.

bis-indoles in 92% (**1u**), 95% (**1v**) and 41% (**1w**) yields respectively. Unexpectedly, the low yield of **1w** is due to the concomitant formation of **1n** in 51% yield by C–C bond cleavage followed by indoloylation of the so-generated indole-3-carboxaldehyde. Furthermore, reactions of ketones with indole were also proceeded satisfactorily, but they needed comparatively longer reaction times and afforded a little lower yield of products than that of aldehydes due to the lower reactivity of ketones. The reaction of ketones such as acetones, butanone, acetophenone and cyclohexanone was allowed individually with simple indole using 2 mol% of $\text{SiO}_2\text{-FeCl}_3$ under grindstone conditions, and the respective bisindolyl products were isolated in 88% (**2a**, 3.5 h), 82% (**2b**, 2.5 h), 94% (**2c**, 4 h) and 92% (**2d**, 1 h) respectively. We have also investigated the catalytic recyclability of the catalyst $\text{SiO}_2\text{-FeCl}_3$ from the reaction of indole and benzaldehyde. After completion of the reaction, the catalyst was filtered by dissolving the products in dichloromethane or ethyl acetate, washed several times, dried under vacuum and used for the next cycle. The results (96%

initial, 95%, 93%, 90% and 90%) evidently showed that the very little loss of catalytic efficiency in each cycle (Fig. 4).

From the careful analysis of the results presented in Table 1, particularly entries 3–6, it is very much clear that the effect of SiO_2 and FeCl_3 is synergic. Thus, we presumed that, both Lewis acid behaviour of FeCl_3 and surface of silica being used in the catalyst are responsible for the catalytic activity. The formation of polynuclear iron(III) complex by the coordination of aldehydic/ketonic carbonyl^{10a} facilitates the nucleophilic attack to the carbonyl center by indole followed by the elimination of water, as silica is a water adsorbent, and then attacks the second molecule of indole reacting with the arylidene/alkylidene moiety so generated after the dehydration process to form bis-indolylmethanes *via* the Michael addition-type process.

Molecular docking study

The world is now facing a serious health crisis due to coronavirus disease (COVID-19) since December 2019. The causative agent for COVID-19 was severe acute respiratory syndrome coronavirus 2 (SARS-CoV-2).³³ Two proteases that facilitate the processing of functional proteins of SARS-CoV-2 are the 3CL^{PRO} and the papain-like protease (PL^{PRO}). 3CL^{PRO} executes proteolytic cleavages at a maximum number of sites (11 sites) within the polyprotein, hence it is also termed the main protease (M^{PRO}). This is a key enzyme of SARS-CoV-2, which plays a pivotal role in mediating viral replication and transcription that make it an attractive drug target to combat COVID-19.³⁴ M^{PRO} are located at the cleft of domains that comprised a His–Cys catalytic dyad (cysteine-145 and histidine-41 residues). Here, cysteine-145 acts as a common nucleophile and plays a major role in the proteolytic functioning of M^{PRO}.³⁵

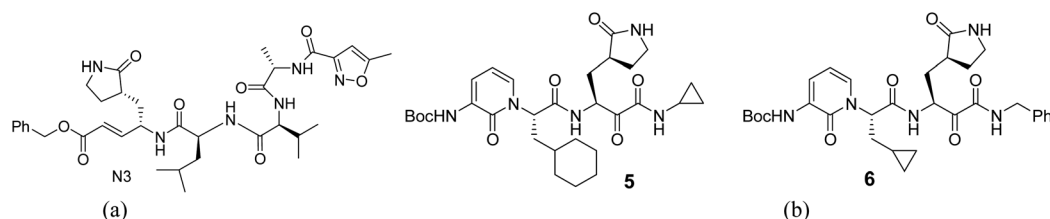


Fig. 5 (a) Structure of the SARS-CoV-2 co-ligand (N3). (b) Structure of known inhibitors 5 and 6.

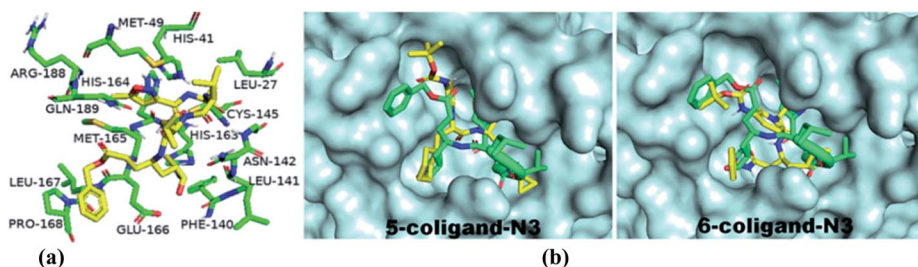


Fig. 6 (a) 3D interactions of the co-ligand with active site amino acid residues of M^{PRO} are depicted by PyMOL in the X-ray crystallographic protein-co-ligand complex of 6LU7. (b) Binding pose of known inhibitors 5 and 6 in the receptor-active site of SARS-CoV-2 M^{PRO} is depicted in PyMOL [structures 5 and 6 (yellow) and co-ligand N3 (green)].

Table 2 The binding affinity (kcal mol^{-1}) was predicted by AutoDock Vina, binding energy (kcal mol^{-1}) was predicted by AutoDock and interacting amino acid residues

Compounds	Binding affinity	Binding energy	K_i (nM)	Interacting amino acid residues
Co-ligand (N3)	-6.6	-7.35	4.07 ^a	Hydrophobic: HIS-41, MET-49, LEU-27, PHE-140, LEU-141, ASN-142, CYS-145, HIS-163, HIS-164, MET-165, GLU-166, LEU-167, PRO-168, ARG-188, GLN-189; H-bonding: GLY-143 (2.97 Å)
5	-7.7	-9.71	76.45	Hydrophobic: THR-25, THR-26, MET-49, PHE-140, LEU-141, ASN-142, CYS-145, HIS-164, MET-165, PRO-168, ASP-187, THR-190; H-bonding: HIS-41 (3.14 Å), GLN-189 (3.11 Å)
6	-7.9	-8.43	664.7	Hydrophobic: HIS-41, MET-49, PHE-140, ASN-142, HIS-164, MET-165, GLU-166, LEU-167, PRO-168, ASP-187, ARG-188, GLN-189; H-bonding: LEU-141 (3.07 Å), GLY-143 (3.13, 3.15 Å), SER-144 (2.81 Å), CYS-145 (3.05 Å), HIS-163 (3.00 Å)
1c	-7.8	-9.05	232.93	Hydrophobic: HIS-41, MET-49, PHE-140, LEU-141, CYS-145, HIS-164, MET-165, GLU-166, ASP-187, ARG-188, GLN-189
1e	-7.6	-8.88	307.65	Hydrophobic: HIS-41, MET-49, PHE-140, LEU-141, CYS-145, HIS-164, MET-165, GLU-166, ASP-187, ARG-188, GLN-189
1f	-7.9	-8.58	515.25	Hydrophobic: HIS-41, HIS-164, HIS-163, LEU-141, ASN-142, GLU-166, MET-165, GLN-189. H-bonding: CYS-145 (3.12), SER-144 (3.16, 2.81), ASN-142 (3.06, 3.18 Å)
1g	-7.3	-9.29	154.54	Hydrophobic: PHE-140, LEU-141, ASN-142, GLY-143, SER-144, CYS-145, HIS-163, HIS-164, MET-165, GLU-166, ARG-188, GLN-189
1l	-7.3	-8.32	794.7	Hydrophobic: MET-49, PHE-140, ASN-142, CYS-145, HIS-164, MET-165, GLU-166, ARG-188, GLN-189
1m	-6.7	-8.31	813.9	Hydrophobic: PHE-140, LEU-141, ASN-142, HIS-164, MET-165, GLU-166, GLN-189. H-bonding: HIS-163 (3.02 Å)
1n	-7.9	-9.13	203.59	Hydrophobic: HIS-41, MET-49, PHE-140, LEU-141, ASN-142, CYS-145, HIS-164, MET-165, GLU-166, ASP-187, ARG-188, GLN-189
1r	-5.8	-6.6	14.35 ^a	Hydrophobic: THR-25, HIS-41, MET-49, PHE-140, LEU-141, ASN-142, CYS-145, HIS-

Table 2 (Contd.)

Compounds	Binding affinity	Binding energy	K_i (nM)	Interacting amino acid residues
1s	-9.1	-12.37	0.8513	163, HIS-164, MET-165, GLU-166, LEU-167, PRO-168, GLN-189 Hydrophobic: THR-199, TYR-237, ASN-238, TYR-239, LEU-271, MET-276, ALA-285, LEU-286, LEU-287; H-bonding: LEU-272 (3.00 Å), ASP-289 (2.85 Å)
1t	-6.0	-8.58	517.49	Hydrophobic: HIS-41, MET-49, LEU-141, ASN-142, CYS-145, HIS-164, MET-165, GLU-166, ASP-187, ARG-188, GLN-189, THR-190; H-bonding: PHE-140 (3.24 Å)
1w	-7.7	-12.27	1.01	Hydrophobic: TYR-239, LEU-286, THR-199; H-bonding: TYR-237 (3.14 Å), LEU-271 (3.27 Å), LEU-272 (2.91 Å), ALA-285 (2.92 Å), LEU-287 (2.80 Å)

^a K_i values expressed in μM .

Recently, Adhikari³⁶ and Sarma³⁷ independently reviewed the anti-SARS effect of some small molecules as 3CLpro inhibitors with their various binding modes of interactions to the target protein for potential remedy of corona virus. Structure-based drug discovery (SBDD) is becoming an essential tool in assisting fast and cost-efficient lead discovery and optimization. Due to the various drawbacks associated with the traditional wet lab screening, the application of the rational drug design approach is proven to be faster and less costly than the traditional high-throughput screening of drug discovery. After successful demonstration of silica-supported ferric chloride in the synthesis of various bis-indolylmethanes and having in mind the efficacy of various indole derivatives, we decided to perform molecular docking studies of the synthesized bis-indole compounds against M^{Pro} . A set of compounds (**1c**, **1e-g**, **1l-n**, **1r**, **1s** and **1w**) were selected keeping in mind their H-bond donor-acceptor ability, π - π interactions capacity and hydrophobicity. The compound **1r** is appended with a long alkyl chain, which is expected to have hydrophobic interactions with the hydrophobic amino acid residues in the active site of the enzyme. However, an amide bond has special features due to the resonance contribution of lone pair of nitrogen to carbonyl group that restrict the C-N rotation by a substantial amount of double bond character, which ultimately provides a geometrically confined structure³⁸ and plays a very important role in biology. Thus, apart from **1r**, we have designed and synthesized another long alkyl chain appended compound **1t** from bis-indolyl methane **1q** on the basis of molecular docking analysis. The nitro group of **1q** was successfully reduced using

hydrazine hydrate-Pd/C (10%) under refluxing in ethanol followed by acylation with dodecanoyl chloride in the presence of Et_3N in dichloromethane at room temperature to afford **1t** in 49% yield (two steps). Molecular docking studies of the compounds were carried out using AutoDock Vina, and AutoDock 4.2.³⁹ The X-ray crystal structures of SARS-CoV-2 life cycle protein M^{Pro} (PDB ID: 6LU7, 2.16 Å) were retrieved from the RCSB protein data bank.⁴⁰ PyMOL (The PyMOL Molecular Graphics System, Version 2.0 Schrödinger, LLC)⁴¹ was used for the visual analysis of protein-ligand complexes and LigPlot+ Version, v.2.2 was used to generate 2D protein-ligand interactions.^{41b} The structures of the synthesized compounds were sketched using Chem Draw Professional 15.1 and were saved as sdf formatted files. Then the structures were imported in Pymol and converted into pdb file format. In the AutoDock Tools interface the pdf formatted files of all the compounds were imported followed by conversion into pdbqt format for compatibility with Autodock 4.2 and Autodock Vina using AutoDock Tools1.5.6.⁴²

The M^{Pro} was imported in AutoDock Tools 1.5.6 and prepared by removal of water, removal of the bound ligand, addition of polar hydrogen atoms followed by computing Gasteiger and adding Kollman partial charges to the protein. Finally, the protein was saved in the pdbqt format. The amino acid residues of 6LU7 from the 5.0 Å distance of the centre of the co-ligand (N3) were LEU-27, HIS-41, HIS-42, LEU-141, GLY-143, GLU-166, PRO-168, ARG-188, THR-190, and GLN-192.

For the docking study, we considered known inhibitor—co-ligand (N3) and two other peptide-based inhibitors **5** and **6** as

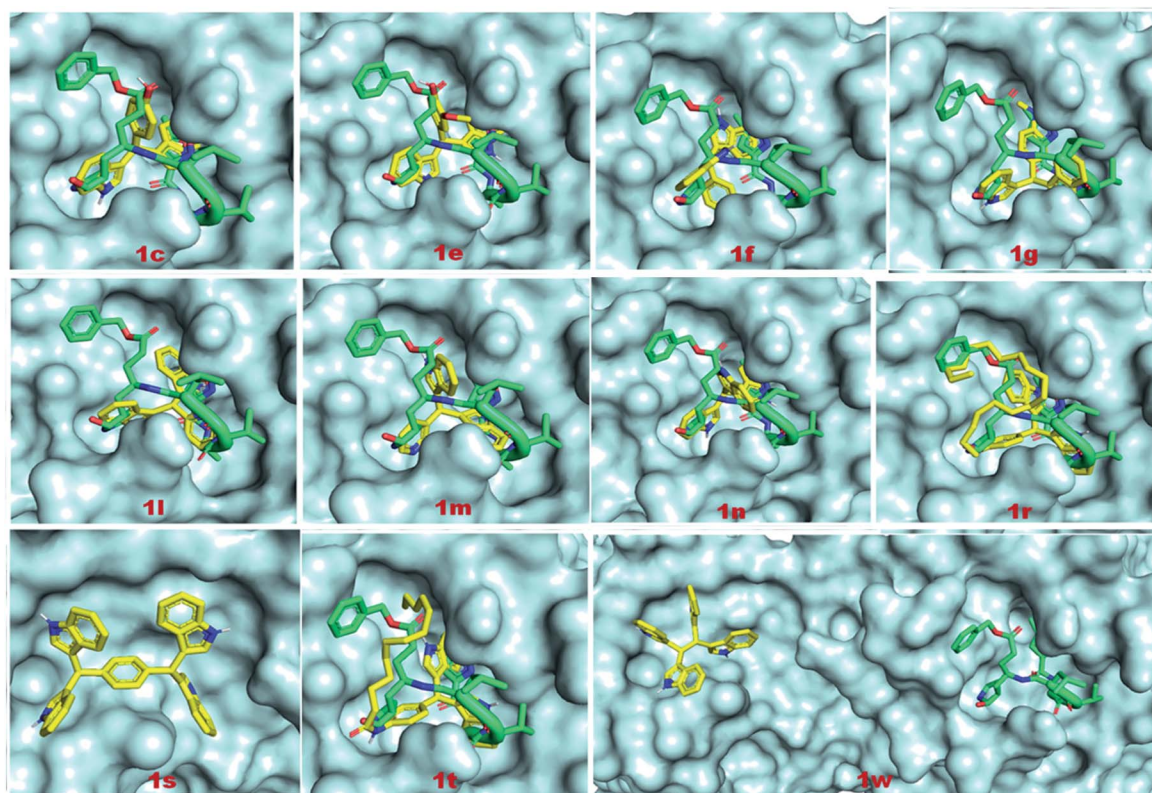


Fig. 7 Binding pose of the eleven compounds **1c**, **1e**, **1f**, **1g**, **1l**, **1m**, **1n**, **1r** and **1t** (yellow) in the receptor-active site and **1s** and **1w** (yellow) in the allosteric site of SARS-CoV-2 M^{PTO} is depicted using PyMOL. Compounds **1s** and **1w** were bounded in a different pocket unlike the co-ligand (green).

reference (Fig. 5). Co-ligand (N3) can specifically inhibit M^{PTO} from multiple coronaviruses, including SARS-CoV and MERS-CoV, and inhibit SARS-CoV-2 replication in human Calu-3 lung cells.⁴³ The active site amino acid residues were selected using PyMOL, and the residues are shown in Fig. 6. The grid centre dimension of M^{PTO} was $x = -10.883$, $y = 13.934$, $z = 68.209$ and grid size was $x = 58$, $y = 68$, $z = 70$. Selecting these residues, a receptor grid was generated. The molecular docking was carried out using Windows 10, OS architecture 64 bit, Core (TM) 2 Due CPU machine.

The binding affinities of coligand (N3) and two known SARS-CoV-2 M^{PTO} inhibitors **5** and **6** were found to be -6.6 , -7.7 and -7.9 respectively, as predicted using AutoDock Vina (Table 2). The binding affinities of the compounds **1c**, **1e**, **1f**, **1g**, **1l**, **1m**, **1n**, **1r**, **1s**, **1t** and **1w** were -7.8 , -7.6 , -7.9 , -7.3 , -7.3 , -6.7 , -7.9 , -5.8 , -9.1 , -6.0 and -7.7 kcal mol⁻¹ respectively, as predicted using AutoDock Vina. The predicted binding affinities of compounds **1c**, **1e**, **1f**, **1g**, **1l**, **1m**, **1n**, **1s** and **1w** were less than the binding affinity of co-ligands (N3). The binding affinities of **1c**, **1f**, **1n**, **1s** and **1w** were less than or equal to the binding affinity of known inhibitor **5**. The binding affinities of **1f**, **1n** and **1s** were less than or equal to the binding affinities of another known inhibitor **6**. The binding energies of coligand (N3) and two known SARS-CoV-2 3CL^{PTO} inhibitors **5** and **6** were -7.35 , -9.71 , and -8.43 kcal mol⁻¹, respectively. The binding energies of the compounds **1c**, **1e**, **1f**, **1g**, **1l**, **1m**, **1n**, **1r**, **1s**, **1w** and **1t** were

-9.05 , -8.88 , -8.58 , -9.29 , -8.32 , -8.31 , -9.13 , -6.60 , -12.37 , -8.58 and -12.27 kcal mol⁻¹ respectively, as predicted using AutoDock. The binding energies of ligands **1c**, **1e**, **1f**, **1g**, **1l**, **1m**, **1n**, **1s**, **1t** and **1w** were less than the binding energy of the co-ligand. The binding energies of **1s** and **1w** were less than the binding energy of known inhibitor **5**. Similarly, the binding energies of **1c**, **1e**, **1f**, **1g**, **1n**, **1s**, **1t** and **1w** were less than the binding energy of another known inhibitor **6**. The docking scores of the ligands **1s** and **1w** were comparatively very good but not bound to the active site of M^{PTO} . Therefore, these two ligands are not considered as good inhibitors. In two docking algorithm, the compounds **1c**, **1e**, **1f** and **1n** showed good binding affinities towards SARS-CoV-2 M^{PTO} . The docking score and interacting amino acid residues of all the compounds, known inhibitors and co-ligands are shown in Table 2. The compounds **1c**, **1e**, **1f**, **1r**, **1g**, **1l**, **1m**, **1n**, **1t**, **5** and **6** bind in the active site region in a similar pose to the X-ray crystallographic bound co-ligand (N3). The binding pose of all the compounds, known inhibitors and co-ligands are shown in Fig. 7. The key amino acid residues that interact with known SARS-CoV-2 M^{PTO} inhibitors identified by MD simulation are HIS-41, GLY-143, and GLU-166.⁴⁴ The compounds **1c**, **1e**, **1f**, **1g**, **1n**, **1r** and **1t** exhibited hydrophobic interactions with at least two residues out of three key interacting residues. The other key interacting amino acid residues of SARS-CoV main protease is CYS-145.⁴⁵ The compounds **1c**, **1e**, **1f**, **1g**, **1l**, **1n**, **1r** and **1t** also showed

hydrophobic interactions with CYS-145. Therefore, except compounds **1s** and **1w** all other compounds showed interactions with key amino acid residues of SARS-CoV-2 M^{Pro}. On the basis of docking scores, interacting amino acid residues and in comparison with co-ligand and known inhibitors, it is concluded that the compounds **1c**, **1e**, **1f** and **1n** may be the potential SARS-CoV-2 M^{Pro} inhibitors (Fig. 8).

Conclusions

In conclusion, we have successfully demonstrated the utility of silica-supported ferric chloride in the synthesis of bisindolyl methane derivatives under grindstone conditions. The catalyst was characterized by SEM/EDX spectra. Our study revealed that the quality of this supported material is retained after six months as well as after recycling several times. The present protocol has several advantages like operational simplicity, shorter reaction time, high yield of the products and tolerance of a wide range of functional groups. We also investigated the molecular docking study of the synthesised compounds by targeting the binding site of SARS-CoV-2 main protease (3CL^{Pro} or M^{Pro}) enzymes. Our study revealed that some of the synthesised compounds could be potential candidates as antiviral agents against SARS-CoV-2 M^{Pro} enzyme as the computational study indicates that some of the synthesised BIM's interacting with key amino acids residues of the active sites by hydrophobic as well as hydrogen bonding interactions.

Experimental section

General method

The starting materials indole or substituted indoles, various types of aldehydes (aromatic, aliphatic, heterocyclic *etc.*), anhydrous ferric chloride and silica gel 230–400 mesh were purchased either from Sigma Aldrich chemical Co., USA or Acros Organics or SRL India and used as received. All the solvents were distilled prior to use. ¹H NMR and ¹³C NMR spectra were recorded at ambient temperature using a Bruker Ascend 400 MHz spectrometer (400 MHz for ¹H and 100 MHz for ¹³C). Chemical shifts were reported in parts per million from the tetramethylsilane internal reference, and coupling constants were reported in Hertz. Proton multiplicities were represented as s (singlet), d (doublet), dd (double doublet), t (triplet), q (quartet), and m (multiplet). Infrared spectra were recorded using a Fourier transform infrared (FT-IR, Model: Spectrum 100) spectrometer KBr pellets or in thin films. The surface morphology of the silica gel-supported material was estimated using a Field Emission Scanning Electron Microscope Model-Sigma 300, Carl Zeiss instrument.

General experimental procedure for the synthesis of 1–2

A mixture of indoles (2.0 mmol), corresponding aldehydes or ketones (1.0 mmol) and FeCl₃·SiO₂ (20 mg, 2 mol% FeCl₃) were taken in a cone-shaped flask and mixed thoroughly using a wide glass rod or spatula. Then, the flask was immersed onto a pre-heated water bath of temperature 80 °C with continuous grinding

of the mixture. After completion of the reaction (monitored by TLC), the catalyst was recovered by dissolving the product in a suitable solvent like ethyl acetate, dichloromethane or methanol. The residue (catalyst) was collected by filtration, dried under vacuum and recycled. The filtrate containing the product was concentrated by distillation under reduced pressure and the distillate was collected for recycling purposes. In most cases, the pure product was crystallized out from the residual filtrate. Only in few cases the product was purified by column chromatography (ethyl acetate–hexane). The synthesized products were characterized by melting point, IR data, NMR, and spectral analysis and compared with the reported compounds. Spectral data of all known compounds are available in ESI.†

3,3'-(4-(Octadecyloxy)phenyl)bis(1H-indole) (1r). Yield: 93%; light orange solid, mp 98–100 °C; FT-IR (KBr) ν_{\max} 3410, 2978, 2310, 1594, 1511, 1391, 1236, 1059, 740 cm⁻¹; ¹H NMR (400 MHz, CDCl₃) δ 7.90 (s, 2H), 7.41 (d, *J* = 8.0 Hz, 2H), 7.37 (d, *J* = 8.0 Hz, 2H), 7.28–7.25 (m, 2H), 7.19 (t, *J* = 6.8 Hz, 2H), 7.02 (t, *J* = 7.6 Hz, 2H), 6.83 (d, *J* = 8.8 Hz, 2H), 6.66 (s, 2H), 5.86 (s, 1H), 3.94 (t, *J* = 6.4 Hz, 2H), 1.78–1.76 (m, 2H), 1.28 (s, 30H), 0.91 (t, *J* = 6.4 Hz, 3H); ¹³C NMR (100 MHz, CDCl₃) δ 157.5, 136.7, 136.0, 129.6, 127.1, 123.5, 121.9, 120.1, 120.0, 19.2, 114.1, 111.0, 68.0, 39.3, 31.9, 29.7, 29.6, 29.5, 29.4, 26.1, 22.7, 14.2. HRMS calcd for C₄₁H₅₄N₂O 590.4236 found 591.4314 (M + H⁺).

3-(1,2,2-Tri(1H-indol-3-yl)ethyl)-1H-indole (1w). Yield: 41% (along with 40% of **1n**), white solid, mp > 250 °C; FT-IR (KBr) ν_{\max} 3249, 3050, 2923, 1618, 1480, 1456, 1345, 1216, 1090 cm⁻¹; ¹H NMR (400 MHz, DMSO-d₆) δ 10.47 (s, 4H), 7.82 (d, *J* = 7.6 Hz, 4H), 7.34 (s, 4H), 7.11 (d, *J* = 7.6 Hz, 4H), 6.90–6.83 (m, 8H), 5.77 (s, 2H); ¹³C NMR (100 MHz, DMSO-d₆) δ 136.2, 127.4, 122.8, 120.5, 119.7, 119.5, 118.1, 111.4, 38.1; HRMS calcd for C₃₄H₂₆N₄ 490.2157 found 492.2246 (M + 2H⁺).

Experimental procedure for the synthesis of 1t from 1q

A mixture of **1q** (367 mg, 1 mmol), Pd-C (10%, 40 mg) and hydrazine hydrate (1.5 mmol) in ethanol (10 mL) was refluxed for 2 h. After cooling, the mixture was filtered off and the residue was washed with ethyl acetate (2 × 10 mL). The combined filtrate was evaporated under reduced pressure and the residue was used for next step without purification. To the stirred solution of the residue in dichloromethane (5 mL), triethylamine (500 μ L) and lauroyl chloride (270 mg, 1.2 mmol) were added successively and stirred for 4 h at room temperature. After completion of the reaction (TLC), water (10 mL) was added and extracted with dichloromethane (3 × 10 mL), dried over anhydrous Na₂SO₄ and evaporated to residue. The purification of the crude product by column chromatography (1 : 1, ethyl acetate–hexane) afforded the title compound **1t**.

N-(4-(Di(1H-indol-3-yl)methyl)phenyl)dodecanamide (1t). Yield: 49% (two steps); pinkish solid, mp 110–112 °C; FT-IR (KBr) ν_{\max} 3396, 2921, 1661, 1597, 1521, 1458, 1409, 1092 cm⁻¹; ¹H NMR (400 MHz, CDCl₃) δ 7.92 (s, 2H), 7.39 (d, *J* = 7.6 Hz, 4H), 7.34 (d, *J* = 8 Hz, 2H), 7.26 (d, *J* = 8.8 Hz, 2H), 7.19 (d, *J* = 7.6 Hz, 2H), 7.16 (s, 1H), 7.01 (t, *J* = 7.6 Hz, 2H), 6.55 (s, 2H), 5.84 (s, 1H), 2.39–2.33 (m, 2H), 1.74–1.66 (m, 2H), 1.28 (bs, 16H), 0.90 (t, *J* = 5.1 Hz, 3H); ¹³C NMR (100 MHz, CDCl₃)

δ 171.5, 140.1, 136.7, 135.9, 129.2, 127.0, 123.7, 121.9, 120.0, 119.9, 119.5, 119.2, 111.1, 39.6, 37.8, 31.9, 29.6, 29.5, 29.4, 29.3, 29.1, 25.7, 24.8, 22.7, 14.1; HRMS calcd for $C_{35}H_{41}N_3O$ 519.3250 found 520.3395 ($M + H^+$).

Conflicts of interest

There are no conflicts to declare.

Acknowledgements

The authors also grateful to Department of Science and Technology (DST), Govt. of India for providing 400 MHz NMR facility under DST-FIST programme (No SR/FST/CSI-263/2015) and Central Instrumentation Centre (CIC) Tripura University from Instrumental facilities.

Notes and references

- (a) I. Eilks and F. Rauch, *Chem. Educ. Res. Pract.*, 2012, **13**, 57–58; (b) C. J. Clarke, W.-C. Tu, O. Levers, A. Bröhl and J. P. Hallett, *Chem. Rev.*, 2018, **118**(2), 747–800; (c) S. A. Matlin, G. Mehta, H. Hopf and A. Krief, *Nat. Chem.*, 2015, **7**, 941–943; (d) R. A. Sheldon, *Green Chem.*, 2005, **7**, 267–278.
- (a) C. Reichardt, *Org. Process Res. Dev.*, 2007, **11**, 105–113; (b) A. Sarkar, S. Satra, S. K. Kundu, A. Hajra, G. V. Zyryanov, O. N. Chupakhin, V. N. Charushin and A. Majee, *Green Chem.*, 2016, **18**, 4475–4525.
- (a) R. R. Hawker and J. B. Harper, *Adv. Phys. Org. Chem.*, 2018, **52**, 49–85; (b) T. Itoh, *Chem. Rev.*, 2017, **117**, 10567–10607; (c) A. S. Amarasekara, *Chem. Rev.*, 2016, **116**, 6133–6183; (d) A. R. Hajipour and F. Refiee, *Org. Prep. Proced. Int.*, 2015, **47**, 249–308.
- (a) B. H. Lipshutz, S. Ghorai and M. Cortes-Clerget, *Chem.–Eur. J.*, 2018, **24**, 6672–6695; (b) R. N. Butler and A. G. Coyne, *Org. Biomol. Chem.*, 2016, **14**, 9945–9960; (c) D. K. Romney, F. H. Arnold, B. H. Lipshutz and C.-J. Li, *J. Org. Chem.*, 2018, **83**, 7319–7322.
- (a) S. Liu, Y. Kumatabara and S. Shirakawa, *Green Chem.*, 2016, **18**, 331–341; (b) L. Zong and C.-H. Tan, *Acc. Chem. Res.*, 2017, **50**, 842–856; (c) D. C. M. Albanese, F. Foschi and M. Penso, *Org. Process Res. Dev.*, 2016, **20**, 129–139; (d) J. Schörghenmer, M. Tiffner and M. Waser, *Beilstein J. Org. Chem.*, 2017, **13**, 1753–1769.
- (a) P. Gracia-Garcia, J. M. Moreno, U. Diaz, M. Bruix and A. Corma, *Nat. Commun.*, 2016, **7**, 10835; (b) M. Kaur, S. Sharma and P. M. S. Bedi, *Chin. J. Catal.*, 2015, **36**, 520–549; (c) S. An, D. Song, B. Lu, X. Yang and Y.-H. Guo, *Chem.–Eur. J.*, 2015, **21**, 10786–10798; (d) F. Su, L. Ma, D. Song, X. Zhang and Y. Guo, *Green Chem.*, 2013, **15**, 885–890.
- (a) R. B. NasirBaig and R. S. Varma, *Chem. Soc. Rev.*, 2012, **41**, 1559–1584; (b) V. Polshettiwar and R. S. Varma, *Acc. Chem. Res.*, 2008, **41**, 629–639.
- (a) A. Stolle, T. Szuppa, S. E. S. Leonhardt and B. Ondruschka, *Chem. Soc. Rev.*, 2011, **40**, 2317–2329; (b) S. Santra, D. S. Kopchuk, I. S. Kovalev, G. V. Zyryanov, A. Majee, V. N. Charushin and O. N. Chupakhin, *Green Chem.*, 2016, **18**, 423–426; (c) A. Khaskel, P. Gogoi, P. Barman and B. Bandyopadhyay, *RSC Adv.*, 2014, **4**, 35559–35567.
- S. Onitsuka, Y. Z. Jin, A. C. Shaikh, H. Furuno and J. Inanaga, *Molecules*, 2012, **17**, 11469–11483.
- (a) S. Majumdar, A. Chakraborty, S. Bhattacharjee, S. Debnath and D. K. Maiti, *Tetrahedron Lett.*, 2016, **57**, 4595–4598; (b) E. Keinan and Y. Mazur, *J. Org. Chem.*, 1978, **43**, 1020–1022; (c) D. Habibi and M. Nasrollahzadeh, *Synth. Commun.*, 2010, **40**, 3159–3167; (d) A. Fadel and J. Salaün, *Tetrahedron*, 1985, **41**, 413–420; (e) M. A. Chari, D. Shobha and K. Mukkanti, *Catal. Commun.*, 2006, **7**, 787–790.
- (a) P. F. Rosales, G. S. Bordin, A. E. Gowar and S. Moura, *Fitoterapia*, 2020, **143**, 104558; (b) T. P. Singh and O. M. Singh, *Mini Rev. Med. Chem.*, 2018, **18**, 9–25.
- F. Zhao, N. Liu, P. Zhan, X. Jiang and X. Liu, *Eur. J. Med. Chem.*, 2016, **94**, 218–228.
- C.-W. Lin, F.-J. Tsai, C.-H. Tsai, C.-C. Lai, L. Wan, T.-Y. Ho, C.-C. Hsieh and P.-D. L. Chao, *Antiviral Res.*, 2005, **68**, 36–42.
- A. K. Ghosh, G. Gong, V. Grum-Tokars, D. C. Mulhearn, S. C. Baker, M. Coughlin, B. S. Prabhakar, K. Sleeman, M. E. Johnson and A. D. Mesecar, *Bioorg. Med. Chem. Lett.*, 2008, **18**, 5684–5688.
- J. Blaising, S. J. Polyak and E.-I. Pecheur, *Antiviral Res.*, 2014, **107**, 84–94.
- M.-Z. Zhang, Q. Chen and G.-F. Yang, *Eur. J. Med. Chem.*, 2015, **89**, 421–441.
- G. M. Ziarani, R. Moradi, T. Ahmadi and N. Lashgari, *RSC Adv.*, 2018, **8**, 12069–12103.
- (a) P. J. Praveena, P. S. Parameswaran and M. S. Majik, *Synthesis*, 2015, **47**, 1827–1837; (b) M. Karthik, A. K. Tripathi, N. M. Gupta, M. Palanichamy and V. Murugeson, *Catal. Commun.*, 2004, **5**, 371–375; (c) M. Chakraborty, N. Ghosh, R. Basak and Y. Harigaya, *Tetrahedron Lett.*, 2002, **43**, 4075–4078; (d) B. P. Bandgar and K. A. Shaikh, *Tetrahedron Lett.*, 2003, **44**, 1959–1961; (e) A. V. Reddy, K. Ravinder, V. L. N. Reddy, T. V. Goud, V. Ravikanth and Y. Venkateswarlu, *Synth. Commun.*, 2003, **33**, 3687–3694.
- (a) M. Xia, S. Wang and W. B. Yuan, *Synth. Commun.*, 2004, **34**, 3175–3182; (b) M. Damodiran, D. Muralidharan and P. T. Perumal, *Bioorg. Med. Chem. Lett.*, 2009, **19**, 3611–3614; (c) G. W. Gribble, *J. Chem. Soc., Perkin Trans. 1*, 2000, **7**, 1045–1075; (d) A. J. K. Karamyan and M. T. Hamann, *Chem. Rev.*, 2010, **110**, 4489–4497; (e) M. Mari, A. Tassoni, S. Lucarini, M. Fanelli, G. Piersanti and G. Spadoni, *Eur. J. Org. Chem.*, 2014, **2014**, 3822–3830; (f) T. Endo, M. Tsuda, J. Fromont and J. Kobayashi, *J. Nat. Prod.*, 2007, **70**, 423–424.
- (a) R. M. F. Batista, S. P. G. Costa, R. M. P. Silva, N. E. M. Lima and M. M. M. Raposo, *Dyes Pigments*, 2014, **102**, 293–300; (b) N. Kumari, S. Jha and S. Bhattacharya, *Chem.–Asian J.*, 2012, **7**, 2805–2812.
- (a) X. He, S. Hu, K. Liu, Y. Guo, J. Xu and S. Shao, *Org. Lett.*, 2006, **8**, 333–336; (b) L. Wang, X. He, Y. Guo, J. Xu and

- S. Shao, *Beilstein J. Org. Chem.*, 2011, 7, 218–221; (c) H. J. Kim, H. Lee, J. H. Lee, D. H. Choi, J. H. Jung and J. S. Kim, *Chem. Commun.*, 2011, 47, 10918–10920.
- 22 R. Martinez, A. Espinosa, A. Tarraga and P. Molina, *Tetrahedron*, 2008, 64, 2184–2191.
- 23 L. Wang, X. He, Y. Guo, J. Xu and S. Shao, *Beilstein J. Org. Chem.*, 2011, 7, 218–221.
- 24 A. C. Lamb, R. A. Federico-Prerez and Z.-L. Xue, *Anal. Biochem.*, 2015, 484, 21–23.
- 25 (a) P. Saini, P. Kumari, S. Hazra and A. J. Elias, *Chem.–Asian J.*, 2019, 14, 4154–4159; (b) D. Xia, Y. Wang, Z. Du, Q.-Y. Zheng and C. Wang, *Org. Lett.*, 2012, 14, 588–591; (c) S. Karmakar, P. Das, D. Ray, S. Ghosh and S. K. Chattopadhyay, *Org. Lett.*, 2016, 18, 5200; (d) R. R. Singh and R.-S. Liu, *Chem. Commun.*, 2017, 53, 4593–4596.
- 26 T. Abe, S. Nakamura, R. Yanada, T. Choshi, S. Hibino and M. Ishikura, *Org. Lett.*, 2013, 15, 3622–3625.
- 27 C.-C. Chen, B.-C. Hong, W.-S. Li, T.-T. Chang and G.-H. Lee, *Asian J. Org. Chem.*, 2017, 6, 426–431.
- 28 (a) B. V. Gregorovich, K. Liang, M. Clugston and S. Macdonald, *Can. J. Chem.*, 1968, 46, 3291–3300; (b) M. Roomi and S. Macdonald, *Can. J. Chem.*, 1970, 48, 139–143; (c) M. El-Sayed, K. Mahmouda and A. Hilgerotha, *Curr. Chem. Lett.*, 2014, 3, 7–14; (d) T. Pillaiyar, M. Dawood, H. Irum and C. E. Müller, *Arkivoc*, 2018, (part iii), 1–19.
- 29 (a) A. Chatterjee, S. Manna, J. Benerji, C. Pascard, T. Prange and J. Shoolery, *J. Chem. Soc., Perkin Trans. 1*, 1980, (1), 553–555; (b) M. Shiri, M. A. Zolfigol, H. G. Kruger and Z. C. Tanbakouchian, *Chem. Rev.*, 2010, 110, 2250–2293; (c) L. Macha, D. Singh, H.-J. Rhee and H.-J. Ha, *Org. Biomol. Chem.*, 2020, 18, 9473–9482.
- 30 (a) M. M. Khodaei, I. Mohammadpoor, H. R. Memarian, A. R. Khosropour, K. Nikofar and P. Ghanbary, *J. Heterocycl. Chem.*, 2008, 45, 1–5; (b) K. Niknam, M. A. Zolfigol, T. Sadabadi and A. Nejati, *J. Iran. Chem. Soc.*, 2006, 3, 31–32; (c) S. Mehrazma, N. Azizi and M. R. Saidi, *Lett. Org. Chem.*, 2006, 3, 161–164; (d) M. Hosseini-Sarvari, *Acta Chim. Slov.*, 2007, 54, 354–359; (e) Z. H. Zhang, L. Yin and Y. M. Wang, *Synthesis*, 2005, 12, 1949–1954; (f) S. J. Ji, M. F. Zhou, D. G. Gu, S. Y. Wang and T. P. Loh, *Synlett*, 2003, 2077–2079; (g) X. Mi, S. Luo, J. He and J. P. Cheng, *Tetrahedron Lett.*, 2004, 45, 4567–4570; (h) V. T. Kamble, B. P. Bandgar and S. N. Bavikar, *Chin. J. Chem.*, 2007, 25, 13–15; (i) P. K. Pradhan, S. Dey, V. S. Giri and P. Jaisankar, *Synthesis*, 2005, 11, 1779–1782; (j) M. Xia, S. H. Wang and W. B. Yuan, *Synth. Commun.*, 2004, 34, 3175–3182; (k) L. P. Mo, Z. C. Ma and Z. H. Zhang, *Synth. Commun.*, 2005, 35, 1997–2004; (l) N.-K. Nguyen, M.-T. Ha, H. Y. Bui, Q. T. Trinh, B. N. Tran, V. T. Nguyen, T. Q. Hung, T. T. Dang and X. H. Vu, *Catal. Commun.*, 2021, 149, 106240 (7 pages).
- 31 (a) M. Chakrabarty, N. Ghosh, R. Basak and Y. A. Harigaya, *Synth. Commun.*, 2004, 34, 421–434; (b) M. L. Deb and P. J. Bhuyan, *Tetrahedron Lett.*, 2005, 47, 1441–1443; (c) M. Karthik, A. K. Tripathi, N. M. Gupta, M. Palanichamy and V. Murugesan, *Catal. Commun.*, 2004, 5, 371–375; (d) G. Penieres-Carrillo, J. G. García-Estrada, J. L. Gutiérrez-Ramírez and C. Alvarez-Toledano, *Green Chem.*, 2003, 5, 337–339; (e) C. Ramesh, J. Banerjee, R. Pal and B. Das, *Adv. Synth. Catal.*, 2003, 345, 557–559; (f) H. A. Soliman, A. Y. Mubarak and S. S. Elmorsy, *Chin. Chem. Lett.*, 2016, 27, 353–358; (g) H. Firouzabadi, N. Iranpoor, M. Jafarpour and A. Ghaderi, *J. Mol. Catal. Chem.*, 2006, 253, 249–251; (h) N. Azizi, L. Torkian and M. R. Saidi, *J. Mol. Catal. Chem.*, 2007, 275, 109–112; (i) T. K. Khatab, A. M. Abdelghany and H. A. Soliman, *Silicon*, 2018, 10, 703–708.
- 32 (a) B. Wu, J. Wen, J. Zhang, J. Li, Y.-Z. Xiang and X.-Q. Yu, *Synlett*, 2009, 500–504; (b) S. S. Shinde, B. S. Chi and D. Y. Lee, *Org. Lett.*, 2008, 10, 733–735; (c) S. A. Siddiqui, U. C. Narkhede, S. S. Palimkar, T. Daniel, R. J. Lahoti and K. V. Srinivasan, *Tetrahedron*, 2005, 61, 3539–3546; (d) G. V. M. Sharma, J. J. Reddy, P. S. Lakshmi and P. R. A. Krishna, *Tetrahedron Lett.*, 2004, 45, 7729–7732; (e) H. J. Park and J. C. Lee, *Synlett*, 2009, 79–80; (f) R. S. Balaskar, B. B. Shingate, M. S. Shingare and D. V. Mane, *Arab. J. Chem.*, 2016, 9, S120–S123; (g) J. Jin, Y. Li, S. Xiang, W. Fan, S. Guo and D. Huang, *Org. Biomol. Chem.*, 2021, 19, 4076–4081.
- 33 (a) C. Huang, Y. Wang, X. Li, L. Ren, J. Zhao, Y. Hu, L. Zhang, G. Fan, J. Xu, X. Gu, Z. Cheng, T. Yu, J. Xia, Y. Wei, W. Wu, X. Xie, W. Yin, H. Li, M. Liu, Y. Xiao, H. Gao, L. Guo, J. Xie, G. Wang, R. Jiang, Z. Gao, Q. Jin, J. Wang and B. Cao, *Lancet*, 2020, 395, 497–506; (b) A. E. Gorbalenya, S. C. Baker, R. S. Baric, R. J. de Groot, C. Drosten, A. A. Gulyaeva, B. L. Haagmans, C. Lauber, A. M. Leontovich, B. W. Neuman, D. Penzar, S. Perlman, L. L. M. Poon, D. V. Samborskiy, I. A. Sidorov, I. Sola and J. Ziebuhr, *Nat. Microbiol.*, 2020, 5, 536–544.
- 34 (a) K. Anand, J. Ziebuhr, P. Wadhvani, J. R. Mesters and R. Hilgenfeld, *Science*, 2003, 300, 1763–1767; (b) V. Grum-Tokars, K. Ratia, A. Begaye, S. C. Baker and A. D. Mesecar, *Virus Res.*, 2008, 133, 63–73.
- 35 A. K. Ghosh, K. Xi, V. Grum-Tokars, X. Xu, K. Ratia, W. Fu, K. V. Houser, S. C. Baker, M. E. Johnson and A. D. Mesecar, *Bioorg. Med. Chem. Lett.*, 2007, 17, 5876–5880.
- 36 B. Adhikari and N. Sahu, *ChemistrySelect*, 2021, 6, 2010–2028.
- 37 M. Konwar and D. Sarma, *Tetrahedron*, 2021, 77, 131761 (20 pages).
- 38 C. R. Kemnitz and M. J. Loewen, *J. Am. Chem. Soc.*, 2007, 129, 2521–2528.
- 39 (a) G. M. Morris, R. Huey, W. Lindstrom, M. F. Sanner, R. K. Belew, D. S. Goodsell and A. J. Olson, *J. Comput. Chem.*, 2009, 6, 2785–2791; (b) O. Trott and A. J. Olson, *J. Comput. Chem.*, 2010, 31, 455–461.
- 40 X. Liu, B. Zhang, Z. Jin, H. Yang and Z. Rao, *RCSB PDB id: 6LU7*, 2020, <https://doi.org/10.2210/pdb6LU7/pdb>.
- 41 (a) L. DeLano, *The PyMOL molecular graphics system*, DeLano Scientific, San Carlos, CA, 2002, <http://www.pymol.org>; (b) R. A. Laskowski and M. B. Swindells, *J. Chem. Inf. Model.*, 2011, 51, 2778–2786.

- 42 M. F. Sanner, *J. Mol. Graph. Model.*, 1999, **17**, 57–61.
- 43 L. Zhang, D. Lin, X. Sun, U. Curth, C. Drosten, L. Sauerhering, S. Becker, K. Rox and R. Hilgenfeld, *Science*, 2020, **368**, 409–412.
- 44 R. Yoshino, N. Yasu and M. Sekijima, *Sci. Rep.*, 2020, **10**, 12493.
- 45 T. Regnier, D. Sarma, K. Hidaka, U. Bacha, E. Freire, Y. Hayashi and Y. Kiso, *Bioorg. Med. Chem. Lett.*, 2009, **19**, 2722–2727.